VIP Zeolite Catalysts Very Important Paper

International Edition: DOI: 10.1002/anie.201505334
German Edition: DOI: 10.1002/ange.201505334

Self-Pillared, Single-Unit-Cell Sn-MFI Zeolite Nanosheets and Their Use for Glucose and Lactose Isomerization

*Limin Ren, Qiang Guo, Prashant Kumar, Marat Orazov, Dandan Xu, Saeed M. Alhassan, K. Andre Mkhoyan, Mark E. Davis, and Michael Tsapatsis**

Abstract: *Single-unit-cell Sn-MFI, with the detectable Sn uniformly distributed and exclusively located at framework sites, is reported for the first time. The direct, single-step, synthesis is based on repetitive branching caused by rotational intergrowths of single-unit-cell lamellae. The self-pillared, meso- and microporous zeolite is an active and selective catalyst for sugar isomerization. High yields for the conversion of glucose into fructose and lactose to lactulose are demonstrated.*

Catalysts with hierarchical porosity consisting of single-or near-single-unit-cell zeolite domains offer, for certain reactions, improved catalytic performance (e.g., higher reaction rate and selectivity, and/or slower deactivation kinetics) compared to that of conventional zeolites.[1,2] For example, Choi et al. demonstrated improved resistance to catalyst deactivation,[3] while Zhang et al. established elimination of diffusion limitations for single-unit-cell, aluminosilicate MFI.[4]

Near-single-or single-unit-cell zeolites can be prepared by pillaring[5] or exfoliation[6] of layered zeolites like MCM-22(P)[7] and multilamellar MFI.[3] They can also be made by direct one-step syntheses using dual templating from surfactant aggregates[8] or functionalized linear polymers.[9] An alternative, one-step, synthesis approach is based on sequential rotational intergrowth,[4,10–12] which under conditions favoring highly anisotropic growth rates, can give zeolite particles consisting of single-unit-cell intergrown zeolite layers.[4] This approach does not require pillaring and/or use of long-chain surfactant or polymeric templating agents and, consequently, it is attractive for its simplicity and low cost. Based on repetitive branching caused by such orthogonal rotational intergrowths of single-unit-cell (2 nm thick along the *b*-axis) MFI lamellae, a predominantly MFI, self-pillared zeolite called SPP (self-pillared pentasil) was prepared in all-silica and aluminosilicate forms, and its adsorption, diffusion and Brønsted acid catalytic performance have been investigated.[4,13–15] The SPP materials were found to be distinct from those of conventional and nanosized MFI.

Herein, we report the one-step synthesis of Sn-containing, self-pillared pentasil (Sn-SPP). We establish by NMR, UV/Vis spectroscopy, and electron microscopy that, for Si/Sn $\approx$200, Sn is present only as framework Sn. We also demonstrate higher yields in mono- and disaccharide isomerizations in comparison to those achieved by conventional micro- and mesoporous materials. Other hierarchical Sn-MFI have MFI domains larger than 1 unit cell[16–18] and, to our knowledge, this is the first time that single-unit-cell Sn-MFI is reported.

Sn-SPP was prepared in a one-step hydrothermal synthesis using tetraethyl orthosilicate (TEOS) as the silica source, tin(IV) chloride pentahydrate or ^{119}tin(II) chloride as the tin source, and commercially available tetrabutylphosphonium hydroxide (TBPOH) as the structure-directing agent (SDA). Three different Sn-SPP materials were prepared with Si/Sn ratios of 75, 186, and 223, and are denoted as Sn-SPP(75), Sn-SPP(186), and ^{119}Sn-SPP(223), respectively (see Supporting Information for details).

Sn-SPP(186) exhibited similar X-ray diffraction (XRD) pattern and Ar-adsorption isotherm with those of Si-SPP (all-silica SPP; Figure 1 a,b), which have been discussed and analyzed before.[4,13] TEM images of Sn-SPP(186) show that its particle size is about 100 nm and composed of lamellae with a layer thickness of 2 nm (corresponds to one-unit-cell along the *b*-axis (Figure 1 c, d)). This morphology is identical to that of typical Si-SPP that has been reported elsewhere, and attributed to rotational intergrowth of single-unit-cell MFI lamellae.[13]

Spatially resolved energy dispersive X-ray (EDX) analysis in scanning transmission electron microscopy (STEM) mode revealed that, with 10–20 nm electron probe steps and coarser, 80–160 nm, averaging, Sn is uniformly distributed, in the SPP particles (Figure 2 a–c and Figure S1 in the Supporting Information). High angle annular dark field (HAADF) STEM imaging was used for examination of Sn distribution with higher resolution. In this method, the image intensity depends on the atomic number (Z) of the elements present in the sample, and can easily reach sub-nm resolution. Sn-SPP(75) shows aggregation of Sn atoms into circular clusters of about 5 nm in size (Figure 2 d and Figure S2a and c) suggesting the presence of extra framework SnO_2 particles. It should be noted that these clusters are too small to be identified in STEM-EDX maps at the current probe steps.

[*] Dr. L. Ren,[+] Dr. Q. Guo,[+] P. Kumar, D. Xu, Prof. K. A. Mkhoyan, Prof. M. Tsapatsis
Department of Chemical Engineering and Materials Science
University of Minnesota
421 Washington Avenue SE, Minneapolis, MN 55455 (USA)
E-mail: tsapatsis@umn.edu
M. Orazov, Prof. M. E. Davis
Chemical Engineering, California Institute of Technology
Pasadena, CA 91125 (USA)
Prof. S. M. Alhassan
Department of Chemical Engineering, The Petroleum Institute
Abu Dhabi (United Arab Emirates)
[+] These authors contributed equally to this work.

Supporting information for this article is available on the WWW under http://dx.doi.org/10.1002/anie.201505334.

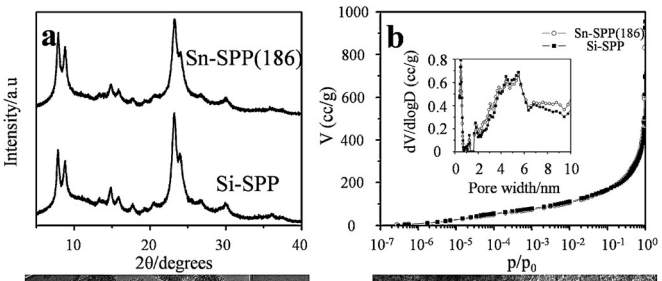

Figure 1. a) XRD patterns and b) Ar adsorption–desorption isotherms (Inset: pore size distribution obtained using NLDFT[19]) of Si-SPP and Sn-SPP(186); c),d) TEM images of Sn-SPP(186). Si-SPP is all-silica SPP and Sn-SPP(186) has aSi/Sn atom ratio of 186 as determined by ICP.

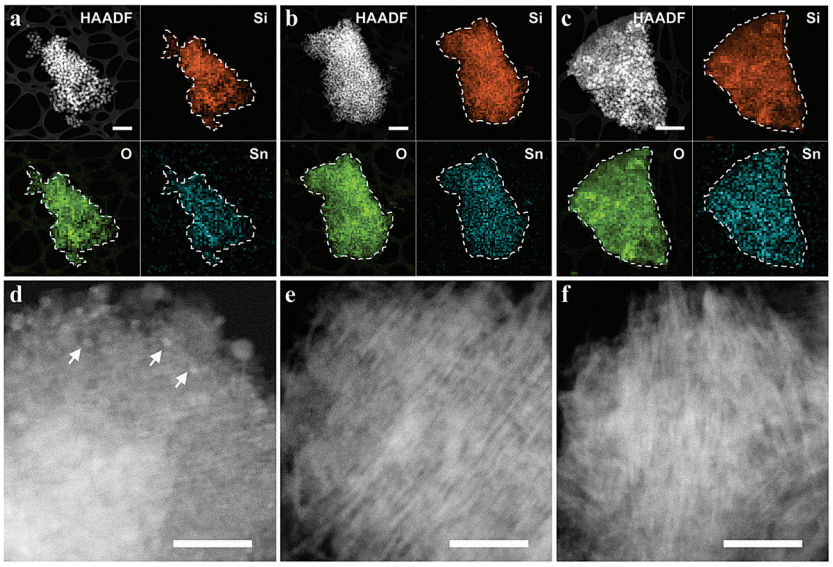

Figure 2. a)–c) EDX-STEM elemental maps along with corresponding HAADF-STEM images from aggregates of around 100 nm individual SPP particles with Si/Sn atomic ratio = 75, 186, and 223, respectively. In elemental maps 8×8 binning is applied to improve signal to noise ratio. Scale bar is 2 μm; d)–f) High-magnification HAADF-STEM images for a single SPP particle with Si/Sn = 75, 186, and 223, respectively. Bright circular aggregates indicated by arrows in (d) are Sn clusters. Scale bar is 40 nm.

Finer resolution STEM-EDX mapping to resolve clusters was unreliable owing to extensive beam damage. Sn-SPP(186) and Sn-SPP(223) show no such clustering of Sn atoms (Figure 2e,f, and Figure S2b,S2d). The microscopy data when taken in total, indicate that increasing the Si/Sn atomic ratio to around 200 reduces Sn clustering to undetectable levels when measured by TEM.

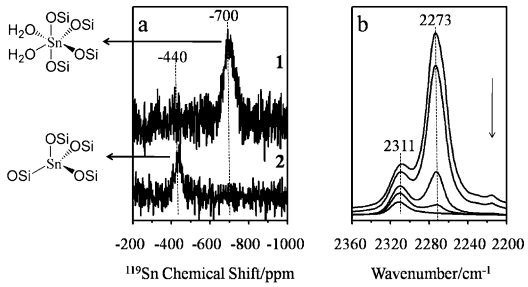

Figure 3. a) ^{119}Sn MAS NMR spectra of 1) hydrated, 2) dehydrated ^{119}Sn-SPP(223); b) IR spectra of deuterated acetonitrile adsorbed on Sn-SPP(186). The arrow indicates desorbing sequence of deuterated acetonitrile in vacuo.

The results from microscopy are in agreement with NMR data, which indicate tetrahedrally coordinated Sn within the zeolite framework upon dehydration (Figure 3a). Specifically, the ^{119}Sn MAS NMR spectrum of the hydrated sample gives a broad signal at −700 ppm (Figure 3a, trace 1), which is assigned to framework octahedral Sn sites coordinated to four framework oxygen and two water molecules.[20,21] After dehydration, a new signal appears at $\delta = -440$ ppm (Figure 3a, trace 2) which is attributed to tetrahedrally coordinated framework Sn[20,21] while the $\delta = -700$ ppm signal for six-coordinate Sn disappears. This behavior and its interpretation are consistent with those of framework Sn in Sn-BEA[20,21] and there was no signal at $\delta = -604$ ppm, excluding the presence of detectable SnO_2. UV/Vis spectra of Sn-SPP(186) and ^{119}Sn-SPP(223) also confirmed that Sn is within the SPP framework (Figure S3). It can therefore be concluded that all detectable Sn (by TEM, NMR and UV/Vis spectroscopy) in Sn-SPP with Si/Sn ≈200 is exclusively located at framework sites.

FT-IR spectroscopy was performed to study the acid properties of Sn-SPP(186) with deuterated acetonitrile as the probe (Figure 3b). Two bands at 2273 and 2311 cm^{-1} are observed, which correspond to the C–N stretching vibration of the adsorbed deuterated acetonitrile.[22] The band at 2273 cm^{-1} arises from the deuterated acetonitrile adsorption on silanol groups and the band at 2311 cm^{-1} dominates at lower deuterated acetonitrile coverage, which can be assigned to the stronger deuterated acetonitrile adsorption on Lewis acid sites.

Sn-SPP was tested as a catalyst for the conversion of glucose (GLU) into fructose (FRU) and compared to several other catalytic materials. The reaction sequence reported in Ref. [23] was followed. According to this scheme (Figure 4a), GLU is first treated in ethanol to give a mixture of FRU (GLU isomerization product) and ethyl fructoside (FRU ketalization product with ethanol). Upon addition of H_2O,

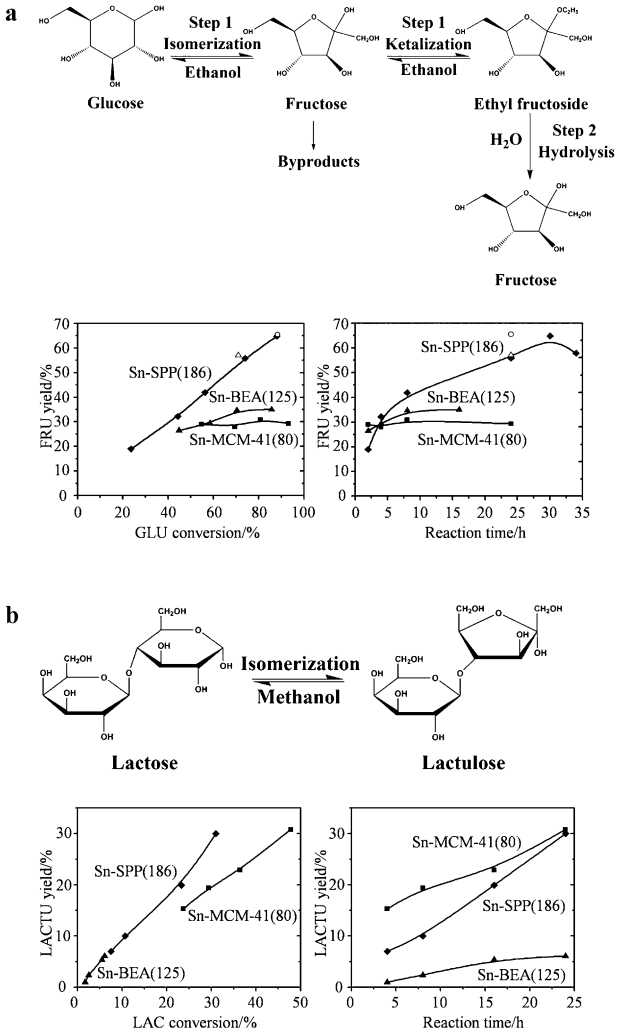

Figure 4. a) Top: Reaction scheme for converting GLU into FRU. Bottom: FRU yield versus GLU conversion and FRU yield versus reaction time over different catalysts; b) Top: Isomerization of LAC to LACTU in methanol. Bottom: LACTU yield versus LAC conversion and LACTU yield versus reaction time over different catalysts. (In (a) and (b) solid diamond: Sn-SPP(186); solid square: Sn-MCM-41(80); solid triangle: Sn-BEA(125); open circle: ^{119}Sn-SPP(223); open triangle: Sn-SPP(75).) Reaction time in (a) is the time for reaction in ethanol before the addition of water (see Supporting Information).

hydrolysis of the fructoside yields FRU. In this approach, it is possible to obtain high yield of FRU if the catalyst can exhibit Lewis and Brønsted acidity to catalyze isomerization, ketalization, and hydrolysis, while allowing sufficient accessibility of the bulky molecules involved to the active sites. It was hypothesized that Sn-SPP should exhibit both Lewis and Brønsted acidity due to framework Sn and surface hydroxy groups, respectively. Indeed, it was found that Sn-SPP(186) was active and selective catalyst for this reaction, achieving approximately 65% FRU yield at about 85% GLU conversion (Figure 4a and Table S2). Similar performance was obtained not only, as expected, for ^{119}Sn-SPP(223) but also for Sn-SPP(75) indicating the presence of framework Sn in Sn-SPP(75) in addition to the SnO_2 clusters detected by TEM. The 65% yield achieved using ethanol as the solvent and reactant for the ketalization is higher than that reported using USY and Al-BEA in methanol and ethanol.[23] Moreover, the corresponding FRU yields for other typical micro- and mesoporous Sn-containing catalysts, that is, Sn-BEA-(125)[24–27] and Sn-MCM-41(80),[24] respectively, were lower as more by-products were detected by HPLC at similar GLU conversions. It appears that the combination of Lewis and Brønsted acidity coupled with facile active-site accessibility are unique characteristics of Sn-SPP.

Sn-SPP is expected to be useful for the conversion of larger substrates. This notion is supported by the results of lactose (LAC) conversion into lactulose (LACTU) shown in Figure 4b and Table S3. The 31% LAC conversion and 97% LACTU selectivity achieved over Sn-SPP(186) in methanol establishes superior performance compared to that of Sn-BEA(125) and Sn-MCM-41(80) as well as earlier reports with micro- and mesoporous catalysts.[18,28]

It was demonstrated that single-unit-cell self-pillared zeolite with framework Sn can be prepared and it has promising catalytic properties. Further investigations regarding the coupling of Lewis and Brønsted acidity and comparisons with other porous catalysts to address the catalytic properties of Sn-SPP will be pursued in future work.

Acknowledgements

This work was supported as part of the Catalysis Center for Energy Innovation, an Energy Frontier Research Center funded by the U.S. Department of Energy, Office of Science, Basic Energy Sciences under Award DE-SC0001004. Q.G.'s postdoctoral fellowship was supported by the Petroleum Institute of Abu Dhabi. We thank Dr. S. Hwang for obtaining solid-state NMR spectra.

Keywords: heterogeneous catalysis · layered materials · nanosheets · self-pillared structures · zeolite

How to cite: *Angew. Chem. Int. Ed.* **2015**, *54*, 10848–10851
Angew. Chem. **2015**, *127*, 10998–11001

[1] M. Tsapatsis, *AIChE J.* **2014**, *60*, 2374–2381.
[2] W. J. Roth, P. Nachtigall, R. E. Morris, J. Čejka, *Chem. Rev.* **2014**, *114*, 4807–4837.
[3] M. Choi, K. Na, J. Kim, Y. Sakamoto, O. Terasaki, R. Ryoo, *Nature* **2009**, *461*, 246–250.
[4] X. Zhang, D. Liu, D. Xu, S. Asahina, K. A. Cychosz, K. V. Agrawal, Y. Al Wahedi, A. Bhan, S. Al Hashimi, O. Terasaki, M. Thommes, M. Tsapatsis, *Science* **2012**, *336*, 1684–1687.
[5] W. J. Roth, C. T. Kresge, J. C. Vartuli, M. E. Leonowicz, A. S. Fung, S. B. McCullen, *Stud. Surf. Sci. Catal.* **1995**, *94*, 301–308.
[6] A. Corma, V. Fornes, S. B. Pergher, T. L. M. Maesen, J. G. Buglass, *Nature* **1998**, *396*, 353–356.
[7] M. E. Leonowicz, J. A. Lawton, S. L. Lawton, M. K. Rubin, *Science* **1994**, *264*, 1910–1913.
[8] K. Na, C. Jo, J. Kim, K. Cho, J. Jung, Y. Seo, R. J. Messinger, B. F. Chmelka, R. Ryoo, *Science* **2011**, *333*, 328–332.
[9] C. Jo, Y. Seo, K. Cho, J. Kim, H. S. Shin, M. Lee, J.-C. Kim, S. O. Kim, J. Y. Lee, H. Ihee, R. Ryoo, *Angew. Chem. Int. Ed.* **2014**, *53*, 5117–5121; *Angew. Chem.* **2014**, *126*, 5217–5221.

[10] A. Inayat, I. Knoke, E. Spiecker, W. Schwieger, *Angew. Chem. Int. Ed.* **2012**, *51*, 1962 – 1965; *Angew. Chem.* **2012**, *124*, 1998 – 2002.
[11] W. Chaikittisilp, Y. Suzuki, R. R. Mukti, T. Suzuki, K. Sugita, K. Itabashi, A. Shimojima, T. Okubo, *Angew. Chem. Int. Ed.* **2013**, *52*, 3355 – 3359; *Angew. Chem.* **2013**, *125*, 3439 – 3443.
[12] M. Khaleel, A. J. Wagner, K. A. Mkhoyan, M. Tsapatsis, *Angew. Chem. Int. Ed.* **2014**, *53*, 9456 – 9461; *Angew. Chem.* **2014**, *126*, 9610 – 9615.
[13] D. Xu, G. R. Swindlehurst, H. Wu, D. H. Olson, X. Zhang, M. Tsapatsis, *Adv. Funct. Mater.* **2014**, *24*, 201 – 208.
[14] P. Bai, D. H. Olson, M. Tsapatsis, J. I. Siepmann, *ChemPhysChem* **2014**, *15*, 2225 – 2229.
[15] G. R. Swindlehurst, P. Kumar, D. Xu, S. M. Alhassan, K. A. Mkhoyan, M. Tsapatsis, *Top. Catal.* **2015**, *58*, 545 – 558.
[16] H. Y. Luo, L. Bui, W. R. Gunther, E. Min, Y. Román-Leshkoy, *ACS Catal.* **2012**, *2*, 2695 – 2699.
[17] H. J. Cho, P. Dornath, W. Fan, *ACS Catal.* **2014**, *4*, 2029 – 2037.
[18] P. Y. Dapsens, C. Mondelli, J. Jagielski, R. Hauert, J. Pérez-Ramírez, *Catal. Sci. Technol.* **2014**, *4*, 2302 – 2311.
[19] P. I. Ravikovitch, A. V. Neimark, *Colloids Surf. A* **2001**, *187 – 188*, 11 – 21.
[20] R. Bermejo-Deval, R. S. Assary, E. Nikolla, M. Moliner, Y. Román-Leshkov, S. J. Hwang, A. Palsdottir, D. Silverman, R. F. Lobo, L. A. Curtiss, M. E. Davis, *Proc. Natl. Acad. Sci. USA* **2012**, *109*, 9727 – 9732.
[21] W. R. Gunther, V. K. Michaelis, M. A. Caporini, R. G. Griffin, Y. Román-Leshkov, *J. Am. Chem. Soc.* **2014**, *136*, 6219 – 6222.
[22] M. Boronat, P. Concepción, A. Corma, M. Renz, S. Valencia, *J. Catal.* **2005**, *234*, 111 – 118.
[23] S. Saravanamurugan, M. Paniagua, J. A. Melero, A. Riisager, *J. Am. Chem. Soc.* **2013**, *135*, 5246 – 5249.
[24] M. Moliner, Y. Román-Leshkov, M. E. Davis, *Proc. Natl. Acad. Sci. USA* **2010**, *107*, 6164 – 6168.
[25] M. Renz, T. Blasco, A. Corma, V. Fornés, R. Jensen, L. Nemeth, *Chem. Eur. J.* **2002**, *8*, 4708 – 4717.
[26] A. Corma, L. T. Nemeth, M. Renz, S. Valencia, *Nature* **2001**, *412*, 423 – 425.
[27] J. Dijkmans, D. Gabriëls, M. Dusselier, F. de Clippel, P. Vanelderen, K. Houthoofd, A. Malfliet, Y. Pontikes, B. F. Sels, *Green Chem.* **2013**, *15*, 2777 – 2785.
[28] R. Gounder, M. E. Davis, *J. Catal.* **2013**, *308*, 176 – 188.

Received: June 11, 2015
Published online: July 23, 2015

